ACCEPTED TO THE ASTROPHYSICAL JOURNAL SUPPLEMENT SERIES
Preprint typeset using LaTeX style emulateapj v. 2/19/04

arXiv:astro-ph/0406035v1 1 Jun 2004

THE 24μm SOURCE COUNTS IN DEEP *SPITZER* SURVEYS[1]

C. PAPOVICH[2], H. DOLE[3], E. EGAMI[2], E. LE FLOC'H[2], P. G. PÉREZ–GONZÁLEZ[2], A. ALONSO–HERRERO[2,4], L. BAI[2], C. A. BEICHMAN[5], M. BLAYLOCK[2], C. W. ENGELBRACHT[2], K. D. GORDON[2], D. C. HINES[2,6], K. A. MISSELT[2], J. E. MORRISON[2], J. MOULD[7], J. MUZEROLLE[2], G. NEUGEBAUER[2], P. L. RICHARDS[8], G. H. RIEKE[2], M. J. RIEKE[2], J. R. RIGBY[2], K. Y. L. SU[2], AND E. T. YOUNG[2]

Accepted to the Astrophysical Journal Supplement Series

ABSTRACT

Galaxy source counts in the infrared provide strong constraints on the evolution of the bolometric energy output from distant galaxy populations. We present the results from deep 24μm imaging from *Spitzer* surveys, which include $\approx 5\times10^4$ sources to an 80% completeness of $\simeq 60$ μJy. The 24μm counts rapidly rise at near–Euclidean rates down to 5 mJy, increase with a super–Euclidean rate between $0.4-4$ mJy, and converge below ~ 0.3 mJy. The 24 μm counts exceed expectations from non–evolving models by a factor $\gtrsim 10$ at $S_\nu \sim 0.1$ mJy. The peak in the differential number counts corresponds to a population of faint sources that is not expected from predictions based on 15μm counts from *ISO*. We argue that this implies the existence of a previously undetected population of infrared–luminous galaxies at $z\sim 1-3$. Integrating the counts to 60 μJy, we derive a lower limit on the 24μm background intensity of 1.9 ± 0.6 nW m^{-2} sr^{-1} of which the majority ($\sim 60\%$) stems from sources fainter than 0.4 mJy. Extrapolating to fainter flux densities, sources below 60 μJy contribute $0.8^{+0.9}_{-0.4}$ nW m^{-2} sr^{-1} to the background, which provides an estimate of the total 24 μm background of $2.7^{+1.1}_{-0.7}$ nW m^{-2} sr^{-1}.

Subject headings: cosmology: observations — galaxies: evolution — galaxies: high–redshift — galaxies: photometry — infrared: galaxies

1. INTRODUCTION

From the first detections of infrared (IR) luminous galaxies, it was clear that they represent phenomena not prominent in optically selected galaxy surveys (e.g., Rieke & Low 1972; Soifer, Neugebauer, & Houck 1987). Locally, galaxies radiate most of their emission at UV and optical wavelengths, and only about one–third at IR wavelengths ($5-1000$ μm; Soifer & Neugebauer 1991). IR number counts from *ISO* indicate that the IR–luminous sources have evolved rapidly, significantly faster than has been deduced from optical surveys, which implies that IR–luminous galaxies make a substantial contribution to the cosmic star–formation rate density (e.g., Elbaz et al. 1999; Franceschini et al. 2001). The detection of the cosmic background by *COBE* at IR wavelengths shows that the total far–IR emission of galaxies in the early Universe is greater than that at optical and UV wavelengths (Fixsen et al. 1998; Hauser et al. 1998; Madau & Pozzetti 2000; Franceschini et al. 2001), which suggests that a large fraction of stars have formed in IR–luminous phases of galaxy activity (Elbaz et al. 2002). Studies from *ISO* at 15 μm and 170 μm have inferred that the bulk of this background originates in discrete sources with $z\lesssim 1.2$ (Dole et al. 2001; Elbaz et al. 2002). However, the peak in the cosmic IR background extends to $\sim 200\mu$m (Fixsen et al. 1998; Hauser & Dwek 2001). The spectral–energy distributions (SEDs) of luminous IR galaxies ($L_{\rm IR}\sim 10^{11-12}\,L_\odot$) peak between $50-80$ μm (Dale et al. 2001). If these objects constitute a major component of the cosmic IR background, then it follows there is a significant population of IR–luminous galaxies at $z\sim 1.5-3$ — distances largely unexplored by *ISO*.

The mid–IR 24 μm band on the Multiband Imaging Photometer for *Spitzer* (MIPS, Rieke et al. 2004) is particularly well suited for studying distant IR–luminous galaxies. Locally, the mid–IR emission from galaxies relates almost linearly with the total IR luminosity over a range of galaxy types (e.g., Spinoglio et al. 1995; Chary & Elbaz 2001; Roussel et al. 2001; Papovich & Bell 2002), and there are indications this holds at higher redshifts (e.g., Elbaz et al. 2002). Because the angular resolution of *Spitzer* is significantly higher for the 24 μm band relative to 70 and 160 μm, the 24 μm confusion limit lies at fainter flux densities. This allows us to probe the IR emission from many more sources and at higher redshifts than with the MIPS longer wavelength bands (e.g., Papovich & Bell 2002; Dole et al. 2003). Here, we present the number counts of $\approx 5\times10^4$ sources detected at 24 μm in deep *Spitzer* surveys, and we suggest that the faint *Spitzer* detections probe a previously undetected population of very luminous galaxies at high redshifts. Where applicable, we assume $\Omega_m=0.3$, $\Omega_\Lambda=0.7$, and $H_0=70$ km s^{-1} Mpc^{-1}.

2. THE DATA AND SOURCE SAMPLES

The data used in this work were obtained in five fields from early *Spitzer* characterization observations and from time allocated to the MIPS Guaranteed Time Observers (GTOs). Table 1 lists their properties and 24 μm source densities. The MIPS fields used here subtend the largest areas ($\simeq 10.5$ deg^2) and widest range in flux density ($50-0.06$ mJy) available to date from the *Spitzer* mission, and therefore are the premier dataset for studying the mid–IR source counts.

[1] This work is based on observations made with the Spitzer Space Telescope, which is operated by the Jet Propulsion Laboratory, California Institute of Technology under NASA contract 1407.

[2] Steward Observatory, The University of Arizona, 933 North Cherry Avenue, Tucson, AZ 85721; Electronic Address: papovich@as.arizona.edu

[3] Institut d'Astrophysique Spatiale, bat 121, Université Paris Sud, F91405 Orsay Cedex, France

[4] Departamento de Astrofísica Molecular e Infrarroja, IEM, CSIC, Serrano 113b, 28006 Madrid, Spain

[5] Michelson Science Center, California Institute of Technology, Pasadena, CA 91109

[6] Space Science Institute, 4750 Walnut, Suite 205, Boulder, CO 80301

[7] National Optical Astronomy Observatory, 950 North Cherry Avenue, Tucson, AZ 85719

[8] Department of Physics, University of California, Berkeley, CA 94720

TABLE 1
PROPERTIES OF DEEP, *Spitzer* FIELDS

Field (1)	R.A. (J2000.0) (2)	Decl. (J2000.0) (3)	$\langle I_\nu \rangle$ (MJy sr^{-1}) (4)	Area (arcmin^2) (5)	$\langle t_{\rm exp} \rangle$ (sec) (6)	$C_{80\%}$ (μJy) (7)	$N(> C_{80\%})$ (arcmin^{-2}) (8)	$N(> 300\ \mu$Jy) (arcmin^{-2}) (9)
Marano	03 13 52	–55 15 23	19.7	1296	236	170	2.0	0.9
CDF–S	03 32 28	–27 48 30	22.5	2092	1378	83	4.5	0.7
EGS	14 16 00	+52 48 50	19.5	1466	450	110	3.4	0.7
Boötes	14 32 06	+34 16 48	22.7	32457	87	270	1.0	0.8
ELAIS	16 09 52	+54 55 00	18.2	130	3232	61	5.7	0.6

NOTE. — Col. (1) Field name; (2) right ascension in units of hours, minutes, and seconds; (3) declination in units of degrees, arcminutes, and arcseconds; (4) mean 24 μm background; (5) areal coverage; (6) mean exposure time; (7) 80% completeness limit; (8) source density with $S_\nu > C_{80\%}$. (9) source density with $S_\nu > 300\ \mu$Jy.

The MIPS 24 μm images were processed with the MIPS GTO data analysis tool (Gordon et al. 2004). The measured count rates are corrected for dark current, cosmic–rays, and flux nonlinearities, and then divided by flat–fields for each MIPS scan–mirror position. Images are then corrected for geometric distortion and mosaicked. The final mosaics have a pixel scale of $\simeq 1\farcs25$ pix^{-1}, with a point–spread function (PSF) full–width at half maximum (FWHM) of $\simeq 6''$.

We performed source detection and photometry using a set of tools and simulations. Briefly, we first subtract the image background using a median filter roughly four times the size of source apertures (see below), and use a version of the DAOPHOT software (Stetson 1987) to detect point sources. We filter each image with a Gaussian with a FWHM that is equal to that of the MIPS 24 μm PSF, and identify positive features in $10''$–diameter apertures above some noise threshold. We then construct empirical PSFs using $20-30$ bright sources in each image, and optimally measure photometry by simultaneously fitting the empirical PSFs to all sources within $\simeq 20''$ of nearby object centroids. The source photometry corresponds to the flux of these PSF–apertures within a diameter of $37\farcs4$, and we apply a multiplicative correction of 1.14 to account for light lost outside these apertures.

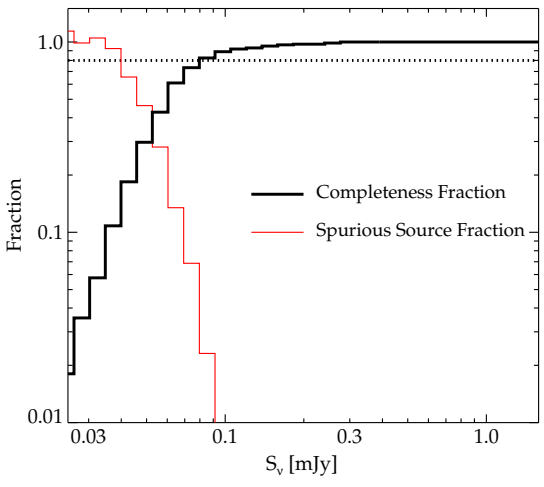

FIG. 1.— Reliability of source detection and photometry for the CDF–S, one of the deep *Spitzer* fields. The *thick* line shows the fraction of artificial sources detected in the image as a function of input flux density. For the CDF–S this fraction is 80% complete at $C_{80\%} = 83\ \mu$Jy (indicated by the *dotted* line). The *red* line shows the ratio of the number of sources detected in a 'negative' of the 24μm image to the number of 'positive' sources as a function of flux density, which provides an estimate of the number of spurious sources due to noise features.

To estimate completeness and photometric reliability in the 24 μm source catalogs, we repeatedly inserted artificial sources into each image with a flux-distribution approximately matching the measured number counts. We then repeated the source detection and photometry process, and compared the resulting photometry to the input values. In figure 1, we show for the *Chandra* Deep Field South (CDF–S; one of the deep, *Spitzer* fields) the relative fraction of sources within $r \leq 2\farcs3$ (half the FWHM) and with a flux difference $< 50\%$ compared to their input values. From these simulations, we estimated the flux–density limit where 80% of the input sources are recovered with this photometric accuracy, and these are listed in table 1. Simultaneously, we estimate that down to the 80% completeness limit the number of sources that result from fainter sources either by photometric errors or the merging of real sources is $\lesssim 10\%$. We also repeated the source detection and photometry process on the negative of each MIPS 24 μm image. This test provides an estimate for the number of spurious sources arising from the noise properties of the image, as shown in figure 1. For all of our fields, the spurious–source fraction for flux densities greater than the 80% completeness limit is $< 10\%$.

3. THE 24 μm SOURCE COUNTS

Figure 2 shows the 24 μm cumulative and differential number counts that have been averaged over the fields listed in table 1. The differential and cumulative counts (corrected and uncorrected) are listed in table 2. The faintest datum (denoted by the open symbol in figure 2) is derived to the 50% completeness limit for the European Large–Area *ISO* Survey (ELAIS) field ($C_{50\%} = 35\ \mu$Jy). The remaining (less deep) fields are used after correcting for completeness to the 80% level only. Error bars in the figure correspond to Poissonian uncertainties and an estimate for cosmic variance using the standard deviation of counts between the fields. For $S_\nu \leq 83\ \mu$Jy where the counts are derived solely from the smaller ELAIS field, we estimate the uncertainty (18%) using the standard deviation of counts at faint flux densities in cells of 130 arcmin^2 from the CDF–S (see below). We have ignored the contribution to the number counts from stars at 24 μm, which are negligible at these Galactic latitudes and flux densities based on preliminary *Spitzer* observations.

At bright flux densities, $S_\nu \gtrsim 5$ mJy, the differential 24 μm source counts increase at approximately the Euclidean

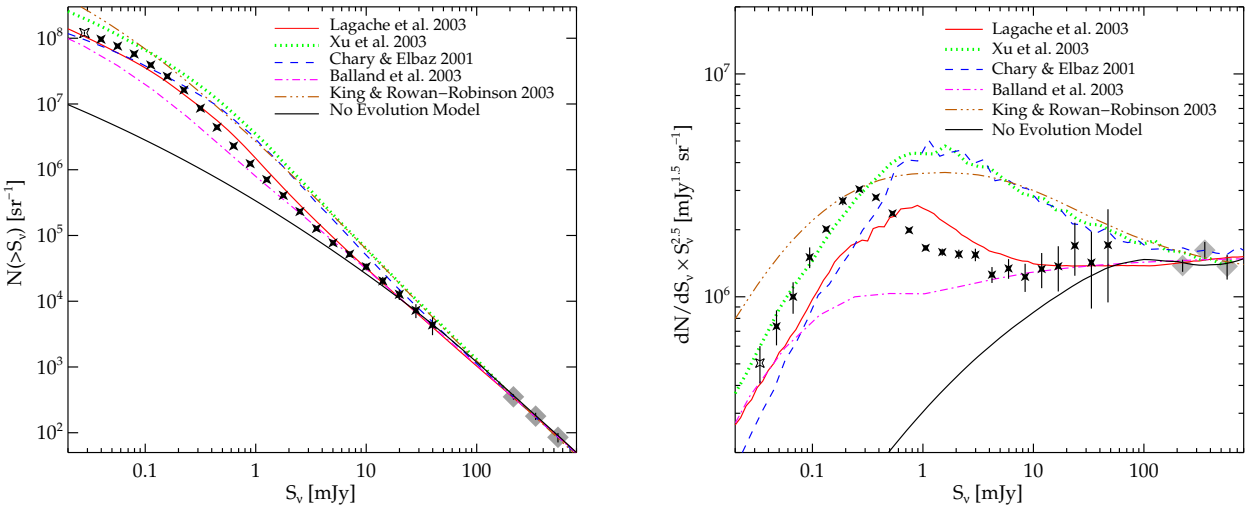

FIG. 2.— Cumulative (*Left* panel) and differential (*Right* panel) 24μm number counts. The differential counts have been normalized to a Euclidean slope, $dN/dS_\nu \sim S_\nu^{-2.5}$. The solid stars show the average counts from all the *Spitzer* fields (see Table 1), and corrected for completeness to their respective 80% limits. The open star corresponds to counts brighter than the 50% completeness limit from the ELAIS field. The error bars correspond to counting uncertainties and a cosmic–variance estimate based on the standard deviation of the field–to–field counts from the different fields. Each flux bin is $\Delta(\log S_\nu) = 0.15$ dex. The shaded diamonds correspond to *IRAS* 25 μm number counts from Hacking & Soifer (1991, and adjusted assuming $\nu_{24}S_\nu(24\mu\mathrm{m}) = \nu_{25}S_\nu(25\mu\mathrm{m})$). The curves show the predictions from various contemporary models from the literature (see figure inset; and adjusted slightly to match the observed *IRAS* counts), and a model based on the local *ISO* 15μm luminosity function and assuming non–evolving galaxy SEDs.

rate, $dN/dS_\nu \sim S^{-2.5}$, which extends the trends observed by the IRAS 25 μm population by two orders of magnitude (Hacking & Soifer 1991; Shupe et al. 1998). For $S_\nu \simeq 0.4-4$ mJy, the 24 μm counts increase at super–Euclidean rates, and peak near $0.2-0.4$ mJy. This observation is similar to the trend observed in the *ISO* 15 μm source counts (Elbaz et al. 1999), but the peak in the 24 μm differential source counts occurs at fluxes fainter by a factor ≈ 2.0. The peak lies above the 80% completeness limit for nearly all fields, and is seen in the counts of the fields individually. Thus the observed turn over is quite robust. The counts converge rapidly with a sub–Euclidean rate at $\lesssim 0.2$ mJy. We broadly fit the faint–end ($S_\nu \simeq 35-130$ μJy) of the differential number counts using a powerlaw, $dN/dS_\nu = C(S_\nu/1\,\mathrm{mJy})^{-\alpha}$, with $\alpha = -1.5 \pm 0.1$. This result is consistent with a separate analysis based solely on the ELAIS field (Chary et al. 2004).

The observed counts are strongly inconsistent with expectations from non–evolving models of the local IR–luminous population. In figure 2, we show the 24 μm counts derived from the local luminosity function at *ISO* 15 μm (Xu 2000) and assuming local galaxy SEDs (Dale et al. 2001). We have used the the local *ISO* 15 μm luminosity function, because the *k*–correction between rest–frame *ISO* 15 μm and observed MIPS 24 μm bands is minimized at higher redshifts ($z \sim 0.6$), which is more appropriate for the counts at fainter flux densities. However, using the local *IRAS* 25 μm luminosity function (Shupe et al. 1998) yields essentially identical results. While the non–evolving fiducial model is consistent with the observed 24 μm counts for $S_\nu \gtrsim 20$ mJy, it underpredicts the counts at $S_\nu \lesssim 0.4$ mJy by more than a factor of 10.

Because the deep *Spitzer* fields are measured in many sightlines with large solid angle, we can estimate the fluctuations in the number of sources as a function of sky area and flux density in smaller–sized fields. For example, in the CDF–S, which achieves an 80%–completeness limit of 83 μJy over $\simeq 0.6$ deg^2 (see table 1 and figure 1), we have computed the variance in the number of sources in solid angles of 100 and 300 arcmin^2. For the sources that span the peak in the differential counts ($0.1-1$ mJy), the fluctuation in the number of sources in flux–density bins of 0.15 dex is roughly 15% in these areas. This implies that small–sized fields suffer sizable field–to–field variation in the number of counts from the cosmic variance of source clustering. This effect is present in even larger fields: the number density of sources brighter than 0.3 mJy varies by $\sim 10\%$ in fields of ~ 0.5 deg^2 (table 1), and is consistent with fluctuations expected from galaxy clustering on fields of this size at $z \sim 1$, (scale lengths of $20-70$ Mpc). The counts presented here average over fields from many sightlines and significantly larger areas. We conservatively estimate that variations due to galaxy clustering correspond to uncertainties in the number counts of a less than a few percent in each flux bin.

4. INTERPRETATION AND DISCUSSION

The form of the observed 24 μm source counts differs strongly from predictions of various contemporary models (see figure 2). Four of the models are phenomenological in approach, which parameterize the evolution of IR–luminous galaxies in terms of density and luminosity to match observed counts from *ISO*, radio, sub–mm, and other datasets. Several of these models (Chary & Elbaz 2001; King & Rowan–Robinson 2003; Xu et al. 2003) show a rapid increase in the number of sources at super–Euclidean rates at relatively bright flux densities ($S_\nu \gtrsim 10$ mJy) and peak near 1 mJy. These models generally predict a redshift distribution for the MIPS 24 μm population that peaks near $z \sim 1$, based largely on expectations from the *ISO* populations, and they overpredict the 24 μm number counts by factors of $2-3$ at ~ 1 mJy. The Lagache et al. (2003) model predicts a roughly Euclidean increase in the counts for $S_\nu > 10$ mJy. The shape of the counts in this model is similar to the observed distribution, but it peaks at $S_\nu \sim 1$ mJy, at higher flux densities than the observed counts. This model predicts a redshift distribu-

tion that peaks near $z \sim 1$, but tapers slowly with a significant population of IR–luminous galaxies out to $z \gtrsim 2$ (Dole et al. 2003).

The model of Balland, Devriendt, & Silk (2003) is based on semi–analytical hierarchical models within the Press–Schecter formalism in which galaxies identified as 'interacting' are assigned IR–luminous galaxy SEDs. This model includes additional physics in that the evolution of galaxies depends on their local environment and merger/interaction histories. Although this model predicts a near–Euclidean increase in the counts for $S_\nu \gtrsim 10$ mJy, the counts shift to sub–Euclidean rates at relatively bright flux densities. The semi–analytical formalism seems to not include important physics that are necessary to reproduce the excess of faint IR sources. This illustrates the need for large–area multi–wavelength studies of *Spitzer* sources to connect optical– and IR–selected sources at high redshift to understand the mechanisms that produce IR–luminous stages of galaxy evolution.

The peak in the 24 μm differential number counts occurs at fainter flux densities than predicted from the phenomenological models based on the *ISO* results. This may suggest possibilities such as a steepening in the slope of the IR luminosity function with redshift, or evolution in the relation between the mid– and total IR. Phenomenological models which reproduce the IR background predict a faint–end slope of the IR luminosity function that should be quite shallow at high redshifts, with 'L^*' luminosities that correspond to $L_{\rm IR} > 10^{11}\,L_\odot$ for $z \gtrsim 1$ (see Hauser & Dwek 2001). For most plausible IR luminosity functions, galaxies with L^* luminosities dominate the integrated luminosity density. Elbaz et al. (2002) observed that the redshift distribution of objects with these luminosities in deep *ISO* surveys spans $z \simeq 0.8-1.2$, and that these objects constitute a large fraction of the total cosmic IR background. Therefore, it seems logical that objects with these luminosities dominate 24 μm number counts at $0.1-0.4$ mJy, and it follows that their redshift distribution must lie at $z \sim 1-3$ (i.e., where this flux density corresponds to $\sim 10^{11-12}\,L_\odot$, using empirical relations from Papovich & Bell 2002). Indeed, a similar conclusion is inferred based on a revised phenomenological model using the 24 μm number counts presented here (Lagache et al. 2004), and allowing for small changes in the mid–IR SEDs of IR–luminous galaxies. Examples of MIPS 24 μm sources at these redshifts and luminosities have been readily identified in optical ancillary data (Le Floc'h et al. 2004). We therefore attribute the the peak in the 24 μm differential number counts at fainter flux densities to a population of luminous IR galaxies at redshifts higher than explored by *ISO*.

Integrating the differential source–count distribution provides an estimate for their contribution to the cosmic IR background at 24 μm, i.e, $I_\nu = \int dN/dS_\nu\, S_\nu\, dS_\nu$. For sources brighter than 60 μJy, we derive a lower limit on the total background of $\nu I_\nu(24\mu{\rm m}) = 1.9 \pm 0.6$ nW m^{-2} sr^{-1}. Due to the steep nature of the source counts, most of this background emission results from galaxies with fainter apparent flux densities. We find that $\simeq 60\%$ of the 24 μm background originates in galaxies with $S_\nu \leq 0.4$ mJy, and therefore the galaxies responsible for the peak in the differential source counts also dominate the total background emission. Our result is consistent with the *COBE* DIRBE upper limit $\nu I_\nu(25\mu{\rm m}) < 7$ nW m^{-2} sr^{-1} inferred from fluctuations in the IR background (Kashlinsky & Odenwald 2000; Hauser & Dwek 2001). As a further estimate on the total 24 μm background intensity, we have extrapolated the number counts for $S_\nu < 60$ μJy using the fit to the faint–end slope of the 24 μm number counts in § 3. Under this assumption, we find that sources with $S_\nu < 60$ μJy would contribute $0.8^{+0.9}_{-0.4}$ nW m^{-2} sr^{-1} to the 24 μm background, which when summed with the above measurement yields an estimate of the total background of $\nu I_\nu^{\rm (tot)}(24\mu{\rm m}) = 2.7^{+1.1}_{-0.7}$ nW m^{-2} sr^{-1}. For this value, the sources detected in the deep *Spitzer* 24 μm surveys produce $\sim 70\%$ of the total 24 μm background.

We acknowledge our colleagues for stimulating conversations, the SSC staff for efficient data processing, Thomas Soifer and the IRS team for executing the Boötes–field observations, Daniel Eisenstein for cosmology discussions, Jim Cadien for his assistance with the data reduction, and the entire *Spitzer* team for their concerted effort. We also thank the referee, Matthew Malkan, for a thorough and insightful report. Support for this work was provided by NASA through Contract Number 960785 issued by JPL/Caltech.

REFERENCES

Balland, C., Devriendt, J. E. G., & Silk, J. 2003, MNRAS, 343, 107
Chary, R. R., & Elbaz, D. 2001, ApJ, 556, 562
Chary, R. R. et al. 2004, ApJS, this issue
Dale, D. A., Helou, G., Contursi, A., Silbermann, N. A., & Kolhatkar, S. 2001, ApJ, 549, 215
Dole, H., et al. 2001, A&A, 372, 364
Dole, H., Lagache, G., & Puget, J.–P. 2003, ApJ, 585, 617
Elbaz, D., et al. 1999, A&A, 351, L37
Elbaz, D., Cesarsky, C. J., Chanial, P., Aussel, H., Franceschini, A., Fadda, D., & Chary, R. R. 2002, A&A, 384, 848
Fixsen, D. J., Dwek, E., Mather, J. C., Bennett, C. L., & Shafer, R. A. 1998, ApJ, 508, 123
Franceschini, A., Aussel, H., Cesarsky, C. J., Elbaz, D., & Fadda, D. 2001, A&A, 378, 1
Gordon, K. et al. 2004, PASP, submitted
Hacking, P., & Soifer, B. T. 1991, ApJ, 367, L49
Hauser, M. G., et al. 1998, ApJ, 508, 25
Hauser, M. G. & Dwek, E. 2001, ARA&A, 39, 249
Kashlinsky, A. & Odenwald, S. 2000, ApJ, 528, 74
King, A. J., & Rowan–Robinson, M. 2003, MNRAS, 339, 260
Lagache, G., Dole, H., & Puget, J.–L. 2003, MNRAS, 338, 555
Lagache, G., et al. 2004, ApJS, this issue
Le Floc'h, E. et al. 2004, ApJS, this issue
Madau, P. & Pozzetti, L. 2000, MNRAS, 312, 9
Papovich, C. & Bell, E. F. 2002, ApJ, 579, L1
Rieke, G. & Low, F. 1972, ApJ, 176, 95
Rieke, G. et al. 2004, ApJS, this issue
Roussel, H., Sauvage, M., Vigroux, L. & Bosma, A. 2001, A&A, 372, 427
Shupe, D. L., Fang, F., Hacking, P. B., & Huchra, J. P. 1998, ApJ, 501, 597
Spinoglio, L., Malkan, M. A., Rush, B., Carrasco, L., & Recillas–Cruz, E. 1995, ApJ, 453, 616
Soifer, B. T., Neugebauer, G., & Houck, J. R. 1987, ARA&A, 25, 187
Soifer, B. T., & Neugebauer, G. 1991, AJ, 101, 354
Stetson, P. B. 1987, PASP, 99, 191
Xu, C. 2000, ApJ, 541, 134
Xu, C., Lonsdale, C. J., Shupe, D. L., Franceschini, A., Martin, C., & Schiminovich, D. 2003, ApJ, 587, 90

TABLE 2
MEASURED *Spitzer* 24 μm NUMBER COUNTS

Log S_ν (mJy) (1)	dN/dS_ν (mJy^{-1} sr^{-1}) (2)	$\delta(dN/dS_\nu)$ (mJy^{-1} sr^{-1}) (3)	Log S_ν (mJy) (4)	$N(>S_\nu)$ (sr^{-1}) (5)	$\delta(N(>S_\nu))$ (sr^{-1}) (6)
–1.475	2.5 (1.4) $\times10^9$	4.7 (1.5) $\times10^8$	–1.550	2.1 (1.1) $\times10^8$	1.2 (0.60) $\times10^7$
–1.325	1.5 (1.2) $\times10^9$	2.7 (0.97) $\times10^8$	–1.400	1.2 (0.92) $\times10^8$	7.6 (4.9) $\times10^6$
–1.175	8.7 (6.9) $\times10^8$	1.4 (1.4) $\times10^8$	–1.250	9.6 (7.2) $\times10^7$	3.7 (0.68) $\times10^6$
–1.025	5.5 (5.2) $\times10^8$	5.8 (1.6) $\times10^7$	–1.100	6.1 (5.6) $\times10^7$	5.9 (5.6) $\times10^5$
–0.875	3.1 (3.1) $\times10^8$	7.1 (4.9) $\times10^6$	–0.950	3.9 (3.9) $\times10^7$	4.0 (4.0) $\times10^5$
–0.725	1.7 (1.6) $\times10^8$	7.6 (6.0) $\times10^6$	–0.800	2.9 (2.5) $\times10^7$	5.5 (5.0) $\times10^5$
–0.575	8.3 (7.5) $\times10^7$	1.5 (0.66) $\times10^6$	–0.650	1.8 (1.6) $\times10^7$	1.8 (1.6) $\times10^5$
–0.425	3.2×10^7	5.7×10^5	–0.500	8.6×10^6	1.2×10^5
–0.275	1.2×10^7	1.9×10^5	–0.350	4.4×10^6	6.2×10^4
–0.125	4.1×10^6	9.6×10^4	–0.200	2.3×10^6	3.8×10^4
0.025	1.4×10^6	3.9×10^4	–0.050	1.2×10^6	2.3×10^4
0.175	5.8×10^5	2.1×10^4	0.100	7.1×10^5	1.7×10^4
0.325	2.4×10^5	1.1×10^4	0.250	4.1×10^5	1.4×10^4
0.475	1.0×10^5	6.5×10^3	0.400	2.3×10^5	1.0×10^4
0.625	3.4×10^4	2.8×10^3	0.550	1.3×10^5	7.1×10^3
0.775	1.5×10^4	1.6×10^3	0.700	7.7×10^4	5.5×10^3
0.925	6.0×10^3	8.6×10^2	0.850	5.2×10^4	7.4×10^3
1.075	2.7×10^3	4.9×10^2	1.000	3.4×10^4	6.0×10^3
1.225	1.2×10^3	2.7×10^2	1.150	2.0×10^4	4.0×10^3
1.375	6.2×10^2	1.7×10^2	1.300	1.3×10^4	2.8×10^3
1.525	2.2×10^2	8.3×10^1	1.450	7.3×10^3	2.1×10^3
1.675	1.1×10^2	5.0×10^1	1.600	4.4×10^3	1.5×10^3

NOTE. — Col. (1) Flux density for differential number counts; (2) Corrected differential counts and (3) uncertainty; (4) Flux density for cumulative number counts; (5) Corrected cumulative counts and (6) uncertainty. Numbers in parentheses give the uncorrected values.